The landscape of PrP^C biosynthesis revealed by an arrayed genome-wide interference screen

Daniel Heinzer[1]*, Merve Avar[1]*, Daniel Patrick Pease[1#], Ashutosh Dhingra[2#], Jiang-An Yin[1], Elke Schaper[1], Berre Doğançay[1], Marc Emmenegger[1], Anna Spinelli[1], Kevin Maggi[1], Andra Chincisan[1], Simone Hornemann[1], Peter Heutink[2], Adriano Aguzzi[1§]

Author affiliations

[1]Institute of Neuropathology, University of Zurich, CH-8091 Zurich, Switzerland

[2]German Center for Neurodegenerative Diseases (DZNE), Otfried-Müller-Str. 23, Tübingen, 72076, Germany.

* # = equal contribution

§ to whom correspondence should be addressed at adriano.aguzzi@usz.ch

Abstract

The availability of the cellular prion protein PrP^C is limiting to prion replication, and its reduction greatly increases life expectancy in animal models of prion infection. Hence the proteins and the biochemical pathways controlling the biosynthesis and the degradation of PrP^C may represent therapeutic targets. Here we performed an arrayed whole-transcriptome RNA interference screen to identify modulators of PrP^C. We cultured human U251-MG glioblastoma cells in the presence of 64'752 unique siRNAs targeting 21'584 annotated human genes, and measured PrP^C using a one-pot fluorescence resonance energy transfer immunoassay in 51'128 individual microplate wells. This screen yielded 743 candidate regulators of PrP^C, which were then filtered through multiple secondary screens. Recursive candidate attrition yielded 54 novel regulators of PrP^C, nine of which emerged as robust regulators of PrP^C biosynthesis and degradation by transcriptional suppression in a CRISPR-interference validation screen. Six candidates were found to regulate PrP^C in the opposite direction when transcriptionally activated using CRISPRa. The RNA-binding post-transcriptional repressor Pumilio-1 was identified as a potent modulator of PrP^C through the degradation of *PRNP* mRNA. Because of its hypothesis-free design, the present listing paints an unbiased landscape of the genes regulating PrP^C levels in cells, most of which were unanticipated, and some of which may be amenable to pharmacological targeting in the context of antiprion therapies.

Introduction

A feature common to all prion diseases is the conversion of the cellular prion protein (PrP^C) into a misfolded, disease-causing isoform called PrP^{Sc} (Aguzzi and De Cecco, 2020). PrP^C is an agonist of the adhesion G protein-coupled receptor Adgrg6 in the peripheral nervous system, but its role in the central nervous system (CNS) has remained unclear (Küffer et al., 2016; Wulf et al., 2017). In prion disease, PrP^C is not only necessary for the generation of PrP^{Sc} but is also involved in mediating neurotoxicity (Brandner et al., 1996). Many lines of evidence indicate that PrP^C is rate-limiting for the progression of prion diseases, and hemizygous *Prnp*$^{+/o}$ mice expressing approximately 60% of wildtype PrP^C levels enjoy a vastly extended life expectancy after prion inoculation (Bueler et al., 1994). Therefore, it was proposed that quenching the availability of PrP^C may represent a feasible therapeutic strategy against prion diseases (Vallabh et al., 2020).

A number of candidate compounds binding to or lowering PrP^C levels have been reported (Karapetyan et al., 2013; Silber et al., 2014). However, small molecules often display pleiotropic actions and off-target

effects, and allosteric interference with protein-protein interactions often requires unrealistically high compound concentrations. Hence, the clinical translatability of such leads has remained challenging. In addition, compounds that lack a well-defined target do not allow drawing far-reaching conclusions about the biosynthesis of PrP^C. Therefore, only few modulators of PrP^C biosynthesis, including the transcription factors sXBP1 and SP1 and the direct interactor, LRP1, were identified thus far (Bellingham et al., 2009; Dery et al., 2013; Parkyn et al., 2008; Rybner et al., 2002; Shyu et al., 2002; Vincent et al., 2009).

Here we have assessed the expression of PrP^C in the human CNS-derived glioblastoma cell line, U251-MG, after downregulation of each protein-coding gene by arrayed RNA interference (RNAi). The screen yielded 54 novel regulators of PrP^C. Nine of those could be validated through an inhibitory CRISPR assay (CRISPRi), and six showed inverted-polarity PrP^C regulation by activating CRISPR (CRISPRa). This unbiased approach enabled the discovery of unanticipated molecular players regulating PrP^C expression levels. The cell-based screening and validation methodologies described here can be easily adapted to identify regulators of the expression of any other protein of interest.

Results

Primary screening for regulators of PrP^C expression

To gain insight into proteins that affect PrP^C expression, we performed a high-throughput whole genome RNAi screen in a human glioblastoma derived cell line, U251-MG. We chose this cell line because it has a relatively high PrP^C expression level and had been successfully utilized in a high-throughput screen for miRNA regulators of PrP^C expression (Pease et al., 2019). We used a commercially available siRNA library consisting of 64’752 unique siRNAs targeting 21’584 annotated human genes. For the primary screening round, three distinct equimolar siRNAs targeting the same transcript were pooled into 21’584 individual wells of 62 plates (1.67 µM per siRNA) to a final concentration of 5 µM. This library was denoted as “pooled library”. Subsequently, siRNAs were reformatted into final assay destination plates to a final concentration of 5 nM using an ECHO555 acoustic dispenser.

We developed a specialized plate layout with the goal of maximizing the randomization of replicas and therefore minimizing the impact of systematic errors. Each assay was run in duplicates dispensed on two individual plates and in two distinct plate locations. We used a cell-death inducing siRNA (20 nM) to control for reduction in viability (n=22 per plate) as well as pool of non-targeting (NT) siRNAs (n=44 per plate, 5 nM)) and a pool of *PRNP*-targeting siRNAs (n=22 per plate, 5 nM). Controls were distributed in a checkerboard pattern across the plate with the aim of identifying any systematic errors deriving from

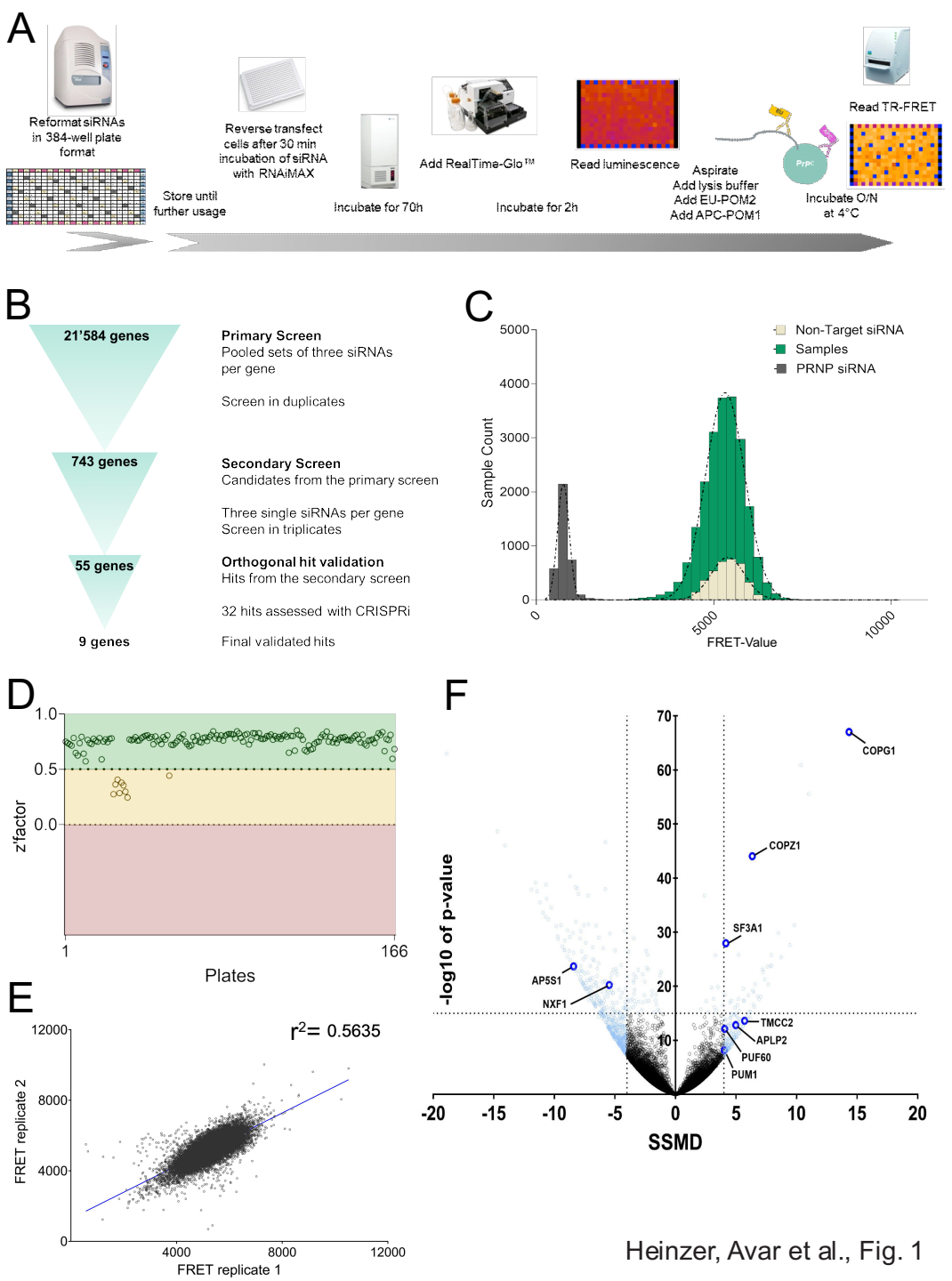

Figure 1. Workflow of the siRNA screen and primary screening round in U251-MG glioblastoma cell line. A) Depiction of the screening workflow. B) Hit selection process. C) Distribution of populations of positive controls (*PRNP* targeting siRNAs), negative controls (non-targeting siRNAs) and samples (contents of whole genome siRNA libraries) across FRET values. The x-axis represents PrP^C levels measured with TR-FRET; the y-axis represents the number of assays grouped for the given FRET range. Controls showed a strong separation allowing a reliable detection of changes in PrP^C levels. Most of the sample population did not show a significant regulation when compared to the non-targeting controls. D) Z' factor of each plate from the primary screen reporting the separability between the positive and negative controls. E) Duplicate correlation over all the samples from the primary screen. The Pearson correlation coefficient, r^2-value, is depicted in the graph. F) Volcano plot displaying $-\log_{10}$p-value and SSMD scores across the whole genome dataset. 743 candidates identified in the primary screen are colored in light blue. Final nine hits are colored in dark blue and labelled.

gradients that may arise in the plates during protracted cell culture (Fig. 1A). Assay plates containing the siRNAs were thawed, and U251-MG cells were seeded following reverse transfection with

Lipofectamine. After three days of culture, cells were lysed and PrP^C levels was measured using a solution-based immunoassay. Two antibodies directed against non-overlapping epitopes of PrP^C, POM2 coupled to Europium (POM2-EU) as donor and POM1 coupled to allophycocyanin (POM1-APC) as acceptor, were added to the lysates. Binding of the antibodies to PrP^C brings the europium and the allophycocyanin into close proximity, allowing for time-resolved fluorescence resonance energy transfer (TR-FRET) and emission of longer-wavelength light whose intensity is proportional to the concentration of PrP^C. For quality control, we first inspected heat maps plotted for raw TR-FRET values per well after correction for spectral overlapping (Ballmer et al., 2017). We then calculated the standardized mean difference (SSMD) and Z' factor (Zhang et al., 1999; Zhang, 2011) reporting the separation of positive (*PRNP* targeting siRNAs) and negative (NT siRNAs) controls.

We measured 166 plates of 384 wells, totaling 63'744 measurements. The outermost wells did not contain any samples and were excluded from Z' factor and SSMD calculations due their proneness for evaporation (Fig. 1C and D and Supplementary Fig. 1A). We considered that inhomogeneities of temperature, humidity or CO_2 concentration during tissue culturing might create artifactual signal gradients which could impair the interpretation of the results. However, no such artifacts were observed across the whole-genome dataset. Z' factors, which report the discriminatory power between positive and negative control, were >0.5 and 0-0.5 for 157 and 9 plates respectively. These values indicate that the screen was robust and allowed for reliable hit calling (Zhang et al., 1999). Inter-plate variability was assessed by calculating the Pearson correlation coefficient between duplicates, and yielded a value of 0.56, indicating that the screen data was sufficiently robust to select candidate genes (Fig. 1E). We used strictly standardized mean differences (SSMD) to assess the effect of each target on PrP^C expression (Zhang, 2011). Targets with an effect size <-4 or >4 on PrP^C expression were considered candidates for a secondary screen. As discordant duplicates occurred rarely (Fig. 1E), they were also included as candidate genes if reaching the threshold of $p > 10^{-15}$ (Student's t-test) which is not sensitive to replica discrepancies.

In summary, out of the 21'584 genes tested, 743 were selected as candidates to be assessed in a secondary screen (SSMD < -4 or > 4 and/or $p > 10^{-15}$ (Supplementary Table 1). When knocked down by siRNA, 563 of these led to a decrease in the PrP^C signal (downregulators) whereas 180 genes increased PrP^C levels (upregulators) (Fig. 1F).

Hit validation through secondary screens

Off-target effects are a common caveat of siRNA screens, and can arise because siRNA seed sequences may display homology to illegitimate loci in the genome (Jackson et al., 2003; Jackson and Linsley, 2010). In order to address this potential problem, we performed a secondary deconvolution screen. Whilst the primary screen had been performed using mixtures of three siRNAs against each gene, in the secondary screen each candidate was subjected to the three targeting siRNAs individually in U251-MG cells. Each experiment was run in three replicates, leading to 9 assays per gene for all 743 candidate genes from the primary screen. The screen was run in two subsets of genes: a first round encompassing 583 genes (Fig. 2A, black dots) and a second round consisting of 160 genes (Fig 2A, purple dots). To add stringency and robustness to this approach, the same single-siRNA screen was performed with a second cell line, GIMEN, which was chosen for its neuroectodermal origin (Kuzyk et al., 2016) and high endogenous PrP^C expression (see Fig. 4B).

Both single-siRNA screens were carried out similarly to the primary screen, except that each assay was run as a triplicate rather than duplicate. Hits were called if ≥2 of the 3 siRNAs had a strong effect (SSMD < -4 or SSMD > 4 or $p < 10^{-15}$). Using these criteria, we identified 54 hits (excluding *PRNP*) in U251-MG cells (Fig. 2A), of which 31 were confirmed in GIMEN cells (Fig. 2B). Out of the 54 hits, 22 and 32 genes were classified as downregulators and upregulators, respectively.

Validation of the hits with siRNAs in smNPC-derived neurons

PrP^C is highly expressed in human neurons (Bendheim et al., 1992), which are key players in prion diseases (Mallucci et al., 2007). We therefore tested the 54 hits in neurons derived *in vitro* from small molecule neural progenitor cells (smNPCs) (Dhingra et al., 2020). Firstly, we assessed the endogenous expression of PrP^C in smNPCs and smNPC-derived neurons at 11 days post differentiation. smNPCs and smNPC-derived neurons showed detectable levels of PrP^C (Supp. Fig. 2B). We then tested the efficiency of siRNA transfection. Four-day old smNPC-derived neurons were transfected individually with three distinct *PRNP* targeting and one non-target siRNAs (10 nM). On day 11, cells were harvested and PrP^C levels were assessed by immunoblotting. The three siRNAs showed variable effects on PrP^C suppression (Supp. Fig. 2C) similarly to the secondary screening, where *PRNP* siRNA 3 also showed the weakest effect.

We then investigated whether the 54 hits identified in the secondary screen produced similar effect in smNPC-derived neurons. We opted to test the effect of each gene by pooling three siRNAs, analogous to the primary whole-genome screen. siRNAs targeting the 54 hits, *PRNP-targeting* siRNAs and non-

targeting siRNA controls were reformatted in a 96-well plate. smNPC-derived neurons were seeded in a separate 96-well plate and cells were transfected with siRNAs after 4 days of differentiation. Seven days later, cells were lysed, and lysates were applied to TR-FRET readout (Fig. 2C). We found that 14 targets showed a conserved effect in smNPC-derived neurons. Of these, 13 were downregulators and one was an upregulator.

CRISPRi validation of hits in dCas9-KRAB U251-MG cells

In order to increase confidence in the hits identified by the secondary screening and to eliminate false-positives due to off-target effects of the siRNAs, we performed CRISPRi experiments in U251-MG cells. We chose CRISPRi as an additional method, as it acts through a repressor domain (KRAB) fused to the Cas9 protein, therefore achieving gene regulation through inhibition of transcription (Qi et al., 2013). Since single clones of dCas9-KRAB-expressing cells can show differential basal transcriptomic

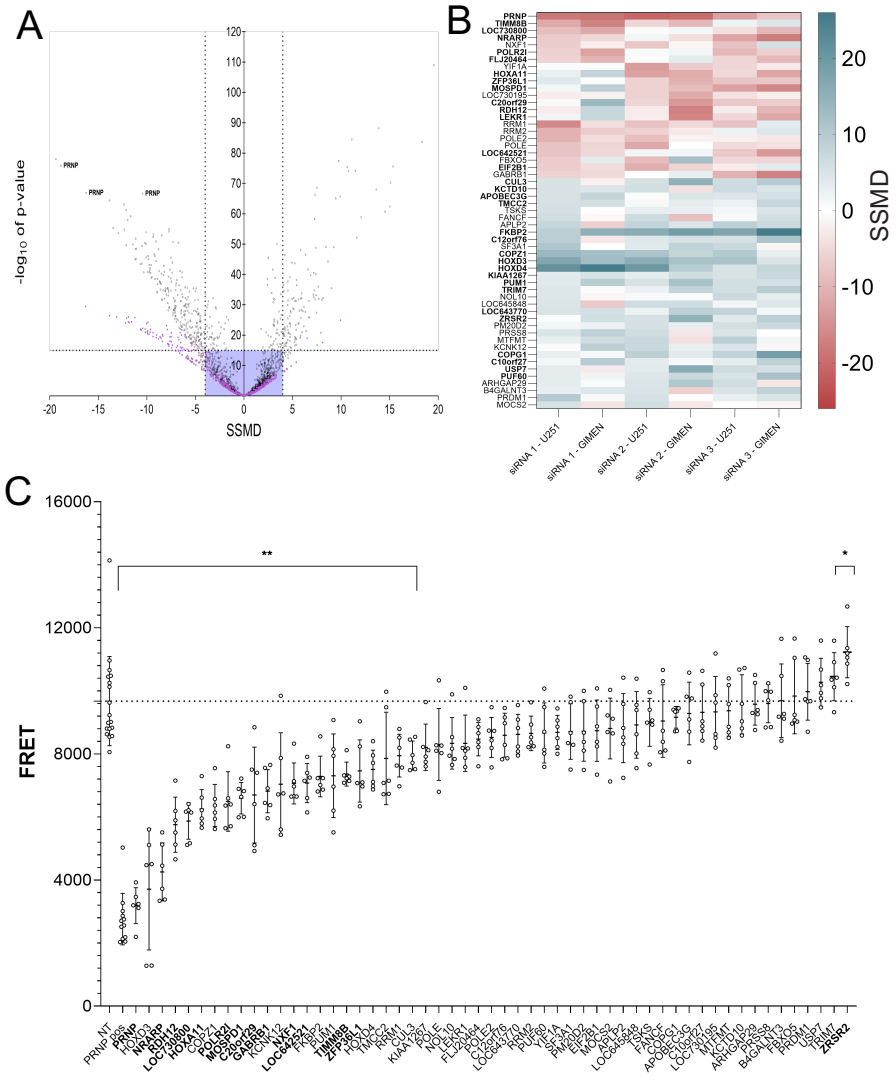

Heinzer, Avar et al., Fig. 2

Figure 2. *Secondary screening and validation of hits in smNPC-derived neurons* **A)** Volcano plot displaying -$\log_{10}$p-value vs. SSMD scores. Three siRNAs per gene were assayed individually. Each dot represents the average of triplicate assays for each individual siRNA; The three different dots representing the three distinct siRNAs for *PRNP* are highlighted. The violet box marks the hit cut-off criteria. Targets with 2 or 3 siRNAs with either SSMD <-4 or >4 or p <10^{-15} were considered hits, yielding 54 hits. Colors indicate screening subsets (black= first round, violet= second round). **B)** Heatmap of the effect size on PrP^C levels for 55 validated hits from the secondary screen. Effect size on PrP^C, measured with SSMD values, are reported for each unique siRNA for U251-MG and GIMEN cell lines. Out of 55 targets, 32 (highlighted in bold) reached the cut-off criteria in GIMEN cells. None of the 55 genes showed opposite effects in the two cell lines. **C)** PrP^C levels in smNPC-derived neurons transfected with a pooled set of siRNAs (as used for the primary screen, 10 nM). Dotted line: average value for cells transfected with non-target siRNAs. Genes highlighted in bold showed the same effect observed in the siRNA screening performed in U251-MG cells. n=6 individual wells for each set of siRNAs. Values represent mean ± SD. * p = 0.0283 ** p ≥ 0.0068 (Dunnett's multiple comparisons test).

signatures (Stojic et al., 2018), we generated a polyclonal bulk of U251-MG$^{dcas9\text{-}KRAB}$ cells through lentiviral transduction and kept it under blasticidin selection (10 μg/mL). Next, we packaged constructs containing guide RNAs (gRNAs) per gene of interest to achieve maximum repression. For controls we used two sets of gRNAs bearing non-targeting sequences with no known homology to any mammalian genes. Positive control contained a construct with gRNAs against *PRNP* (Supplementary Fig. 2A).

A total of 32 genes were further assessed with CRISPRi. We opted to exclude 22 candidates from further analysis based on low abundance of transcripts in the U251-MG line or known global regulators of protein production (expression data summary can be found in Supplementary Table 2). We seeded $2x10^5$ U251-MG$^{dCas9\text{-}KRAB}$ cells in 6-well plates and transduced them on the next day with lentiviruses containing gRNAs for each of the candidate genes. At 3 days post transduction, we selected the transduced cells with puromycin (1 μg/mL) for 5 further days (Supplementary Fig. 2B). Lysates were then subjected to either TR-FRET to assess PrP^C levels or quantitative real-time PCR (qRT-PCR) to determine the efficiency of the CRISPRi treatment (list of all primers used in the study can be found in Supplementary Table 3). CRISPRi yielded efficient downregulation of 27 candidates after 5 days of selection (Fig. 3A, Supplementary Fig. 2C). *NXF1*, a nuclear export factor involved in mRNA export (Chen et al., 2019) did not yield an apparent downregulation potentially due to its interference with the house keeping gene, however, PrP^C levels were altered. Ten of the 32 tested hits were found to regulate PrP^C in CRISPRi experiments (Fig. 3A and Supp. Fig. 2C).

Mechanism of action of PrP^C regulators

The hits described here may regulate PrP^C by affecting its transcription, its translation, or its turnover. In order to distinguish between these scenarios, we challenged the ten hits once more with CRISPRi, to additionally assess mRNA levels of *PRNP* using qRT-PCR, in combination with PrP^C levels by western blotting and TR-FRET. This final selection round yielded APLP2, TMCC2, C20orf29/AP5S1, SF3A1, COPZ1 and COPG1 as post-translational regulators of PrP^C. Instead, PUM1, PUF60 and NXF1 were found to regulate PrP^C by altering *PRNP* mRNA levels (Fig. 3B, Supplementary Fig. 2D). Interestingly, the band pattern on the western blot for NXF1, PUF60, COPZ1, COPG1 and SF3A1 CRISPRi samples revealed to have an effect on the glycosylation of PrP^C (Fig. 3C). We conclude that CRISPRi induced highly efficient and selective repression of select genes, thereby representing a valid tool for the independent confirmation of the results obtained from RNAi experiments.

CRISPRa validation of hits in dCas9-VPR U251-MG cells

To assess whether an opposing regulation could be achieved through the activation of the final 9 hits, we performed CRISPRa. In contrast to a repressor domain used in CRISPRi experiments, the endonuclease deficient Cas9 (dCas9) in this instance is coupled to a transcriptional activator domain, VP64-p65-RTA (VPR), leading to efficient activation of target genes (Chavez et al., 2015) . In a similar setup to the CRISPRi experiments, we generated a polyclonal bulk of U251-MG$^{dCas9\text{-}VPR}$ cells and later transduced these cells using gRNAs targeting the nine hits. We included *PRNP* targeting control gRNAs as well as scrambled non-targeting gRNA sequences. Differentially to the CRISPRi experiments, CRISPRa led to an efficient upregulation of *PRNP* on protein and RNA levels already at three days post-selection (Supplementary Fig. 3A, 3B and 3C). All 9 hits were efficiently upregulated in mRNA levels as measured by qRT-PCR (Supplementary Fig. 3D) with at least one construct targeting different TSS. TMCC2, APLP2, PUM1, COPG1, COPZ1 and SF3A1 led to regulation of PrP^C measured with TR-FRET and visualized with immunoblotting in the opposing direction to the CRISPRi results (Supplementary Fig. 3E, 3F), suggesting these 6 hits have a bidirectional effect on PrP^C levels.

PUM1 mediates decay of PRNP through binding its 3`UTR

One of the 9 hits was Pumilio-1 (PUM1), an RNA-binding protein that binds its targets through their 3'-untranslated Region (3'-UTR) and mediates their decay (Van Etten et al., 2012). PUM1 binds its targets through a well-established consensus sequence, the Pumilio responsive element (PRE, 5'-UGUANAUA-3') (Bohn et al., 2018). We first tested whether the PRE was present on the 3`UTR of *PRNP*. Using the RPI-Seq tool (Muppirala et al., 2011), we identified a PRE within the 3`UTR of *PRNP*. To confirm that PUM1 is a regulator of *PRNP* mRNA, we performed independent siRNA transfections in 6-well plates in both cell lines, U251-MG and GIMEN. We then subjected the extracted RNA to real-time quantitative PCR (qRT-PCR) and cell lysates to immunoblotting. In both cell lines tested, we confirmed that PUM1 silencing had an upregulating effect on *PRNP* mRNA, which also resulted in higher protein levels (Fig. 4A-B).

We then used a dual-luciferase reporter assay to test whether the effect observed was due to the predicted interaction of PUM1 with the 3'-UTR of *PRNP* mRNA. The wild-type (wt) and a mutated (mut) version of the *PRNP* 3'-UTR were cloned into pmirGLO vectors encoding Renilla and Firefly luciferase. These two enzymes report transfection efficiency and activity of the inserted construct, respectively. The

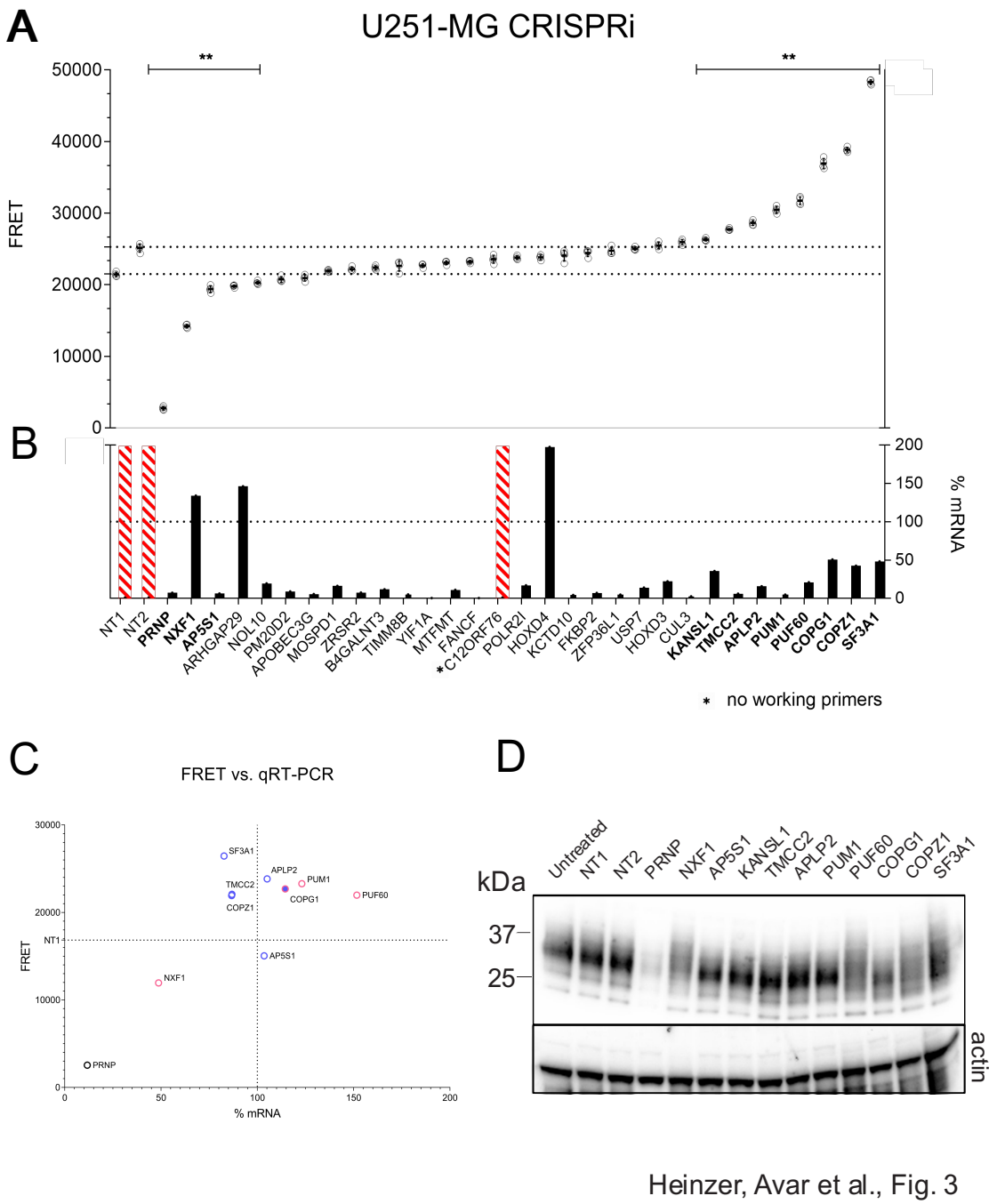

Figure 3. *Hit validation in U251-MG cells by CRISPR interference*. **A)** PrP^C protein levels of dCas9KRAB-U251-MG cells transduced with gRNA CRISPRi lentiviruses against the targets depicted in B. Mean values ± SD (n=4 technical replicates) are shown. ** $p \geq 0.0023$ (Dunnett's multiple comparisons test). **B)** CRISPRi activity measured by the mRNA level of the target gene in comparison to a negative control sample (NT1) after normalization to the housekeeping gene *ACTB*. *C12orf76* could not be tested due to non-functional primers. Three targets showed an increase in mRNA levels, and 27 genes showed the expected decrease in mRNA levels. Two constructs bearing non-targeting gRNAs were used for control. Only genes which showed a statistically significant difference to both NTs were considered to be true hits. Hits with same directionality and effect obtained in the siRNA screens are highlighted in bold. Bars represent averages of three replicates. **C)** qRT-PCR analysis of *PRNP* mRNA of the nine confirmed hits with a significant effect on PrP^C levels. Normalization to *ACTB*. Three genes (pink) regulated *PRNP* mRNA levels, whereas five (blue) modulated PrP^C levels post-transcriptionally and one gene (pink circle with blue filling) acted both transcriptionally and post-translationally. **D)** Western blot analysis of the same 10 samples as in B, probed with antibody POM2 against PrP^C. The FRET and immunoblot results were congruent. In addition, NXF1, PUF60, COPZ1, COPG1 and SF3A1 induced a shift in the glycosylation pattern of PrP^C.

mutation induced spanned three base pairs (bp) of the PRE on *PRNP* 3'-UTR to impair the binding of PUM1 as previously reported (Kedde et al., 2010). Plasmids were then transfected into HEK293T cells

in presence or absence of either NT or PUM1 targeting siRNAs. Luminescence arising from the Firefly luciferase was measured after 48 hours and was followed by the measurement of Renilla luciferase for normalization. In the absence of siRNAs as well as in presence of NT siRNA treatment the mutated 3'-UTR containing construct yielded a higher signal in comparison to the wt 3'-UTR containing construct.

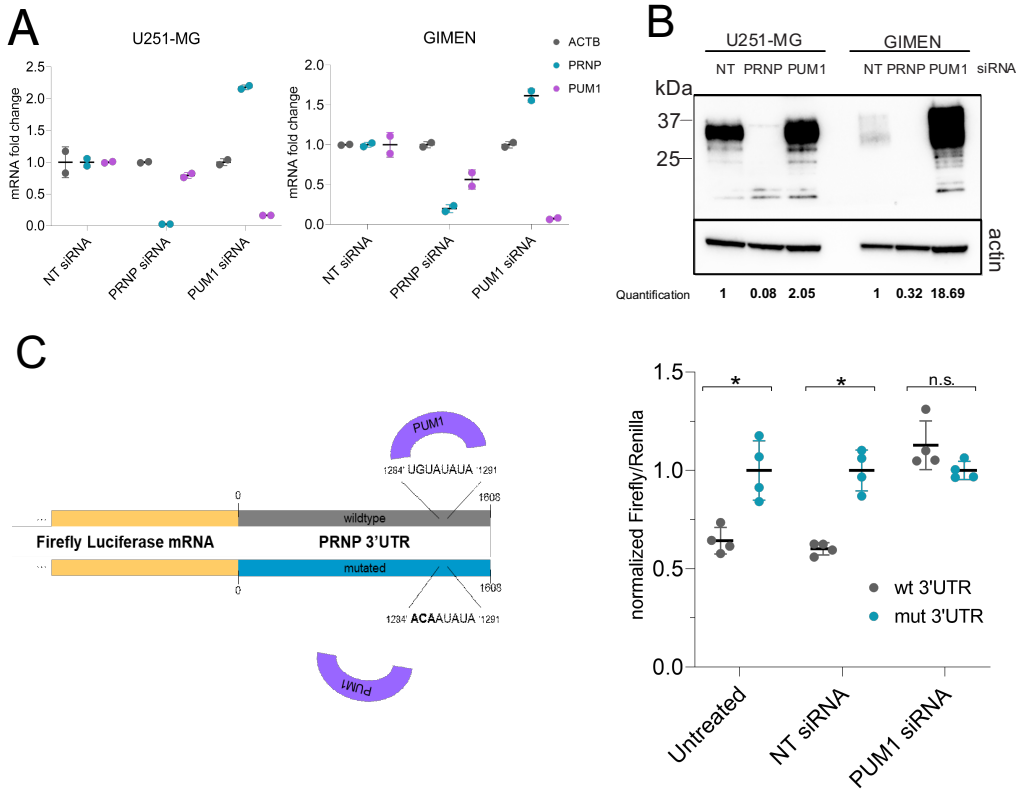

Heinzer, Avar et al., Fig. 4

Figure 4. *PUM1 regulates PRNP mRNA via its 3'UTR*. **A)** qRT-PCR analysis of U251-MG and GIMEN cell lines upon transfection with *PUM1* siRNA in 6-well format. *PUM1* mRNA was efficiently downregulated. ΔCt values were normalized to those of β-actin (*ACTB*). Downregulation of *PUM1* resulted in increased *PRNP* mRNA in both cell lines. *PRNP* siRNA was used for control. **B)** Western blot analysis of U251-MG and GIMEN cell lines upon transfection with *PUM1* siRNA. *PUM1* downregulation lead to an upregulation of PrP^C levels (as seen in Fig. 3B through CRISPRi). Antibody POM2 was used for detection of PrP^C. *PRNP* siRNA was used for control. For quantification, signal intensity of PrP^C was normalized to the signal intensity of β-actin **C)** Dual-Glo Luciferase assay to assess regulation of *PRNP* mRNA by *PUM1* via its 3'-UTR. Left panel shows a schematic of the assay. The numbers indicate the position in the 3'-UTR of *PRNP*. The *PRNP* 3'-UTR sequence, predicted to bear the consensus sequence for *PUM1* binding, was placed after the gene coding for the firefly luciferase. Through a mutation in the 3'-UTR binding site of *PUM1* (wt 3'-UTR => mut 3'-UTR), the binding is prevented leading to increased expression of the firefly luciferase. Two plasmids (wt 3'-UTR and mut 3'-UTR) were co-transfected into HEK293-T cells either with none, NT, or *PUM1* siRNAs. Cells transfected with the mut 3'-UTR plasmid showed a higher signal in the assay in comparison to transfection with the wt 3'UTR plasmid. Similar results were obtained for co-transfection of mut 3'-UTR plasmid and a non-targeting siRNA. The co-transfection with *PUM1* siRNA abrogated the signal difference. Means ± SD (n=4). * $p \leq 0.016$, n.s. = non-significant (multiple t-test).

When cells were treated with PUM1 targeting siRNAs the difference seen in the decrease in signal for the wild-type construct was abolished, indicating that PUM1 is indeed acting on the 3'-UTR of *PRNP* mRNA (Fig. 4C).

Discussion

The concentration of PrP^C in any given cell type is the expression of an equilibrium between its biosynthesis and degradation rates, which in turn are controlled by a multitude of processes – from mRNA transcription to co-translational secretion into the endoplasmic reticulum, quality control of folding, glycolipid bonding, vesicular transport, and eventually proteolysis as well as extracellular shedding. Most factors controlling these steps are unknown, and it is difficult to imagine that they could be discovered through educated guesses. Conversely, an unbiased interrogation of the entire human genome would yield PrP^C regulators that may not have been predicted by existing knowledge.

As *PRNP* is highly expressed in the CNS (Bendheim et al., 1992), we chose a glioblastoma cell line U251-MG for the initial round of screening, additionally due to the suitability of this cell line in high-throughput screenings (Pease et al., 2019). Our strategy relied on recursive screening rounds leading to progressive attrition of candidates. The primary screening campaign, in which each gene was targeted with a mixture of 3 siRNAs, identified 743 presumptive candidate genes strongly influencing PrP^C levels. However, a secondary screen with individual siRNAs showed that many of these hits could only be confirmed with one or two of the three siRNAs present in the original mixtures. These discrepancies may arise because the efficacy of suppression by the individual siRNAs was variable, or because some siRNAs exerted spurious off-target effects. We therefore decided to perform tertiary screens on those candidates that showed an effect with at least 2 siRNAs in two different cell lines. This filtering strategy represents a trade-off between the elimination of false-positive signals and the retention of assay sensitivity.

The resulting list of 54 genes was then interrogated further to assess their effect on human neurons differentiated in vitro. These investigations confirmed most of the hits identified as PrP^C downregulators, but only one upregulator gene. The bias towards downregulators may be a consequence of the long half-life of proteins in post-mitotic neurons (Dörrbaum et al., 2018) which may conceal the effects of short RNAi regimens, and suggests that most downregulators may directly affect *PRNP* biosynthesis. We addressed these questions by suppressing the genes of interest with an independent methodology. CRISPRi has recently emerged as a potent tool to reliably control gene expression (Gilbert et al., 2013; Qi et al., 2013). We used multiple gRNA sequences per target, with the intent to increase the efficiency of modulation (Kurata et al., 2018). Through CRISPRi we identified nine hits significantly regulating PrP^C, six of which controlled PrP^C levels post-translationally.

The partial discordance between the results obtained through siRNAs and CRISPRi is not unexpected. Firstly, the mode-of action of the methods chosen are distinct from each other. In our setup, we applied siRNAs for a duration of three days, which leads to an acute depletion of the target mRNAs, however, to achieve efficient CRISPRi, the cells were cultured for eight days, during which compensatory mechanisms controlling gene expression may take place. Secondly, the use of two non-targeting controls for CRISPRi as opposed to one non-targeting control for siRNAs increases the stringency for calling hits. Thirdly, potential off-target effects seen through one of the methods can be distinct from the other.

Because of the reasons expounded above, the nine genes identified in both approaches represent, with a high degree of confidence, true regulators of PrP^C. To explore if the regulation of PrP^C by the final hits occurs bidirectionally, we made use of a second system, CRISPRa, relying on an endonuclease deficient Cas9 coupled to a transcriptional activator domain (Chavez et al., 2015). We found that 6 of the 9 hits acted in an opposing direction on PrP^C levels, upon their activation with CRISPRa. One of the latter hits, Pumilio 1 (PUM1), is a known mediator of degradation of transcripts through binding to the 3'UTR on their mRNA (Van Etten et al., 2012). *PRNP* was not identified in a previous study of PUM1-regulated genes (Bohn et al., 2018), perhaps because of insufficient levels of PrP^C expression in HEK cells. Sequence inspections then revealed the PUM1-binding consensus sequence in the human, but not mouse, *Prnp* 3'UTR, and mutational analyses of the consensus sequence confirmed the mechanism of this regulation. Besides clarifying the molecular mechanism by which PUM1 modulates PrP^C, these data provide direct evidence for the validity of the regulators identified in our screen.

We failed to identify any transcription factors specifically controlling PrP^C expression in the CNS, perhaps because transcriptional gene regulation relies on redundant factors. Also, the cancer cell line used for the primary screen, while derived from a CNS tumor, may not be representative of transcriptional regulation within the CNS.

Some of the regulators identified in this screen were not entirely unexpected. The members of the COPI complex, COPG1 and COPZ1, are involved in the retrograde transport of vesicles from the Golgi apparatus to the ER. Interference with the COPI complex is known to affect the expression of membrane proteins such as APP (Bettayeb et al., 2016). Furthermore, AP5S1 is part of the newly described Fifth Adaptor Protein Complex (AP-5) which recycles proteins out of late endosomes (Hirst et al., 2011). The decrease of PrP^C after AP5S1 knockdown may be due to decreased retrieval from late endosomes.

Other regulators were entirely unexpected, and their mechanism of action is not obvious. The ablation of APLP2 had no significant effect on incubation times of scrapie in mice (Tamgüney et al., 2008), suggesting that the upregulation of PrP^C upon APLP2 knockdown may be specific to humans. Mechanistically, APLP2 might serve as a co-receptor for the endocytosis of PrP^C, akin to what has been described for MHC class I molecules (Peters et al., 2013) Alternatively, the regulation of PrP^C may be related to the role of APLP2 in metal homeostasis (Millhauser, 2004; Roisman et al., 2019). TMCC2 has been previously described as an ER-resident molecule that interacts with APP and has an effect on metabolism of amyloid-β (Hopkins et al., 2011). In view of the analogies between prion diseases and Alzheimer's disease (Aguzzi and Haass, 2003), the regulation of PrP^C via TMCC2 may occur through a common mechanism. NXF1 and PUF60, well known RNA-regulating proteins, may directly influence the availability of *PRNP* mRNA. Finally, in the case of SF3A1, a splicing factor, the regulation of PrP^C may be indirect as there are no known mechanisms by which SF3A1 could interfere with the formation of PrP^C at the protein level. To extend the understanding of the regulatory network of PrP^C expression, we also cross-referenced the nine hits to miRNAs hits previously identified by our group (Pease et al., 2019). The study identified four miRNA targets for which no direct interaction with *PRNP* mRNA was established. However, based on the target prediction data, miRDB, (Chen and Wang, 2020) we did not find any plausible links between the identified miRNA hits and the nine hits reported here.

In addition to the mechanisms discussed above, the biogenesis of PrP^C involves co-translational secretion of the nascent polypeptide chain into the lumen of the ER and addition of a glycophosphoinositol (GPI) anchor. However, not all of the players known to control these processes were identified as hits. For one thing, some of these genes encode essential proteins whose knockdown may drastically decrease cell viability. Furthermore, because the pathways involved in proteostasis are multiple and partially redundant (Andréasson et al., 2019), suppressing a single gene may not result in a measurable effect on PrP^C levels.

In many neurodegenerative diseases, including Alzheimer's and Parkinson's disease, fundamental clues to the pathogenesis were provided by the study of families with Mendelian disease transmission. However, in the case of prion diseases these strategies have been largely unsuccessful. Although genome-wide association studies (GWAS) have identified two potential risk loci (Jones et al., 2020), the only strong genetic risk factor for Creutzfeldt-Jakob disease has remained *PRNP* itself (Hsiao et al., 1989). This sobering situation was a primary driver of the present study, as the assessment of every individual protein-coding gene may plausibly highlight factors undetectable by human genetics. Indeed,

the modifiers enumerated here provide unexpected insights into a vast and highly diverse regulatory network of PrP^C. PrP^C suppression is a promising strategy for carriers of pathogenic *PRNP* mutations (Minikel et al., 2020; Raymond et al., 2019), and some of the factors identified here might be druggable with the intent to reduce PrP^C levels.

Material and Methods

Cell culturing

U-251MG (Kerafast, Inc., Boston, MA, USA, AccessionID: CVCL_0021) and GIMEN (CLS Gmbh, Eppelheim, Germany AccessionID: CVCL_1232) cells were cultured in T150 tissue culture flasks (TPP, Trasadingen, Switzerland) in OptiMEM without Phenol (Gibco, Thermo Fisher Scientific, Waltham, MA, USA) supplemented with 10%FBS (Takara, Göteborg, Sweden), 1% NEAA (Gibco), 1% GlutaMax (Gibco), and 1% Penicilin/Streptomycin (P/S) (Gibco). HEK293-T cells (AccessionID: CRL_3216) were cultured DMEM without phenol (Gibco) with the same conditions for aforementioned supplements. In preparation for the screening, cells were expanded, either harvested using Trypsin-EDTA 0.025% (Gibco) or Accutase (Gibco), washed with PBS (Kantonsapotheke, Zurich, Switzerland) and resuspended in Penicilin/Streptomycin free medium, pooled, and counted using TC20 (BioRad) Cell Counter with trypan blue (Gibco). Culturing of the cells for the smNPC-derived neurons was done using a published protocol (Dhingra et al., 2020).

siRNA library preparation and reformatting

Whole genome Silencer Select Human Genome siRNA Library V4 (Thermo Fisher Scientific), which includes three individual siRNAs targeting each gene (64752 total siRNAs targeting 21.584 human genes) was purchased at the quantity of 0.25 nmol. Upon delivery, the lyophilized library was resuspended in RNAse free water (Thermo Fisher Scientific) to a final concentration of 5 µM. siRNAs targeting the same gene were aliquoted in a single transfer step using ViaFlo equipment (Integra, Konstanz, Germany) either as pooled siRNAs (referred to as the pooled library) targeting the same gene or as single siRNAs (referred to as the single library) into ECHO acoustic dispenser (Labcyte, San Jose, CA, USA) compatible 384-well LDV plates (Labcyte). For the primary screen, pooled siRNAs and control siRNAs were dispensed in duplicates at a final concentration of 5nM (20 nM for Cell Death control, Qiagen, Hilden, Germany) into white 384-well CulturPlates (Perkin Elmer, Beaconsfield, UK) using an ECHO 555 acoustic dispenser according to an optimized plate layout (Pease et al., 2019) and stored at -40°C until further use. For the secondary screen, individual siRNAs were dispensed in triplicates. As

controls, a scrambled non-targeting siRNA (NT) (Ambion, Thermo Fisher Scientific) as negative and a PRNP targeting siRNA (Ambion, Thermo Fisher Scientific) as positive control, were reformatted to destination plates either as three siRNAs in pooled format or as single siRNAs. All siRNA sequences are accessible under the PubChem repository, NCBI (PubChem, 2013).

Screening workflow

Cell culture plates containing reformatted siRNAs were thawed and 5 µL RNAiMAX (Invitrogen, Carlsbad, CA, USA) (1.8% v/v, final conc. 0.3%) diluted in P/S free medium was dispensed using a multi-drop dispenser (MultiFlo FX, Biotek, Vinooski, VT, USA). Plates were centrifuged at 1000xG for 1 minute (Eppendorf 5804R, Hamburg, Germany) and incubated for 30 min at room temperature (RT). Afterwards, 6'000 cells (U251-MG) or 8'000 cells (GI-ME-N) per well were seeded in 25 µL P/S free medium and plates were incubated in a rotating tower incubator (LiCONiC StoreX STX, Schaanwald, Liechtenstein). For the primary screen, plates were removed from the incubator after 70 hours and 10 µL of 4x RT-Glo substrate and enzyme per well (Promega, Madison, WI, USA) diluted in P/S free medium, was added. Plates were incubated for another 2 hours in the incubator. Prior to measuring luminescence temperature of EnVision plate reader (Perkin Elmer) was set to 37°C and luminescence was measured without disturbances in temperature. Subsequently, medium was removed by inverting the plates, and cells were lysed in 10 µL lysis buffer (0.5% Na-Deoxycholate (Sigma Aldrich St. Louis, MO, USA) 0.5% Triton X (Sigma Aldrich), supplemented with EDTA-free cOmplete Mini Protease Inhibitors (Roche, Basel, Switzerland) and 0.5% BSA (Merck, Darmstadt, Germany). Following lysis, assay plates were incubated on a plate shaker (Eppendorf ThermoMixer Comfort) for 10 min (4°C, 700 rpm shaking conditions) prior to centrifugation at 1000xG for 1 min and incubated at 4°C for two additional hours. Following incubation, plates were centrifuged once more under same conditions mentioned above and 5 µL of each FRET antibody pair was added (2.5 nM final concentration for donor and 5 nM for acceptor, diluted in 1x Lance buffer, (Perkin Elmer)). For FRET, two distinct anti-PrP antibodies, POM1 and POM2 (Polymenidou et al., 2008), targeting different epitopes of PrP^{C} were coupled to a FRET donor, Europium (EU) and a FRET acceptor, Allophycocyanin (APC), respectively, following previously reported protocols (Ballmer et al., 2017). For APC – POM1 coupling, Lightning-Link APC Labeling Kit (Lucerna Chem, Lucerne, Switzerland) was used following manufacturer`s instructions. Plates were centrifuged once more and incubated overnight at 4°C. TR-FRET measurements were read out using previously reported parameters (Ballmer et al., 2017) on an EnVision multimode plate reader (Perkin Elmer).

Screening data analysis

Screening data was analyzed using an in-house developed, open-source, Phyton-based high throughput screen (HTS) analysis pipeline (all documentation and code available under: https://github.com/elkeschaper/hts). Net-FRET data was calculated (Ballmer et al., 2017) and subjected to various quality control checkpoints. Initially, a heat map of individual plates was plotted to examine temperature-induced gradients or dispensing errors. Subsequently, z'-Factor and strictly standardized mean difference (SSMD) scores (Zhang et al., 1999; Zhang, 2011) were calculated to report the robustness of the screens. Additionally, Net-FRET values were plotted to check for row or column effects as well as assessing correlation of duplicates or triplicates. After assessing quality of each individual plate, candidate genes were selected with the following cut-off criteria: SSMD of < -4 and > 4 *or* a p-value (t-test) of below 10^{-15}. After the secondary screen, same cut-off criteria were used with the additional requirement at least 2 out of 3 individual siRNAs targeting the same transcript passing the threshold. Graphs were generated with GraphPad Prism.

PUM1 validation and reporter assay

U251-MG or GI-ME-N cells were seeded into 6- well cell culture plates in a total culture volume of 1.5 mL. Next days, cells were transfected with NT or PUM1 siRNAs (Thermo Fisher Scientific) to a final concentration of 5 nM in a total culture volume of 2 mL. 72 hours post-transfections cells were washed once in PBS to remove cell debris and collected for immunoblotting and quantitative real-time polymerase chain reaction (qRT-PCR). For immunoblottings, cells were scraped with 100 µL lysis buffer (50 mM Tris-HCl pH 8, 150 mM NaCl, 0.5% sodium deoxycholate, 0.5% Triton-X 100, Sigma) supplemented with EDTA-FREE cOmplete Mini protease inhibitor cocktail (Sigma), incubated on ice for 20 minutes and centrifuged at 10.000xG for 10 minutes for isolation of proteins. Supernatants were then subjected to bicinchoninic acid assay (Pierce, Waltham, MA, USA) to measure total protein concentrations according to manufacturer's instructions. 25 µg of total proteins of all samples were loaded onto a 4-12% gradient gel (Invitrogen) and blotted onto a PVDF membrane (Invitrogen). Following blocking in 5% SureBlock reagent (LubioScience, Zurich, Switzerland) diluted in PBS-Tween20 (PBST, Sigma) for 30 minutes, anti-PrP antibody POM2 (Polymenidou et al., 2008) was applied to the membrane at a final concentration of 300 ng/mL in 1% SureBlock in PBST and incubated overnight at 4°C. As a detection antibody anti-Mouse HRP (BioRad) was used diluted 1:10.000 in 1% SureBlock containing PBST. Immunoblots were developed with Crescendo HRP substrate (Millipore, Dachstein, France). As loading control, an anti-Actin antibody m25 (Merck) was used at a dilution of

1:10.000 in 1%Sureblock containing PBST. Imaging was performed on Vilber (Eberhardzell, Germany) systems. Quantification was done with ImageLab (BioRad) For qRT-PCR, cells were lysed in 350 µL RLT lysis buffer (Qiagen) and RNA was extracted using RNeasy Mini kit (Qiagen) manufacturer's instructions. Concentration and quality of RNA was assessed using a NanoDrop spectrophotometer (Thermo Fisher Scientific). cDNA synthesis was done following the manufacturer's instructions using the Quantitect Reverse Transcription kit (Qiagen). A total of 25 ng of cDNA per sample was manually transferred into 384-well PCR plates (Thermo Fisher Scientific) and SYBR green (Roche) mastermix was used for detection. Readout was performed with ViiA7 Real Time PCR systems (Thermo Fisher Scientific). As internal controls, three housekeeping genes (ACTB, TBP, GUSB) were measured for each sample. Data was analyzed and visualized using GraphPad Prism.

Wild-type 3'UTR of PRNP (1608 base pairs (bp)) and a mutant version thereof, were ordered as gene blocks (Integrated DNA Technologies (IDT), Newark, NJ, USA). The mutation was positioned at the PUM1 binding site 5'-TGTATATA-3', where TGT was exchanged to ACA in line with previous reports (Kedde et al., 2010). Additionally, the sequence was modified to contain an overlap of 25 bp at the 5' end and 21 bp at the 3' end with the pmirGLO Dual-Luciferase miRNA Target Expression Vector for molecular cloning into pmirGLO Dual-Luciferase miRNA Target Expression Vector (Promega). The pmirGLO vector was initially digested with PmeI (New England Biolabs (NEB), Ipswitch, MA, USA) and SalI (NEB). Either the wild-type or the mutant version of the *PRNP* 3'UTR were inserted into the digested pmirGLO vector by performing a Gibson Assembly following manufacturer`s instructions (NEB). After transformation of the cloned vectors and purification of the DNA using EndoFree Plasmid Maxi Kit (Qiagen), the purified products were sent to Microsynth AG (Balgach, Switzerland) for Sanger sequencing and aligned to reference sequence of 3`UTR of PRNP using Nucleotide-Blast (NCBI). Final constructs were designated as wild-type (wt)-3`UTR-pmirGLO or mutant (mut)-3`UTR-pmirGLO.

$1x10^4$ HEK-293T cells were seeded in culture medium without antibiotics in white 96-well culture plates (Perkin Elmer) prior to transfection. 100 ng of the wt/mut- 3'UTR-pmirGLO plasmid and 1 pmol of PUM1 or NT siRNAs (Thermo Fisher Scientific) were co-transfected in quadruplicates for each condition using 1% Lipofectamine 2000 (Thermo Fisher Scientific). Four additional wells contained no siRNAs. 48 hours post-transfection, the Dual-Glo Luciferase Reagent (Promega) was added to each well and the luminescence of the firefly luciferase was measured using EnVision plate reader (Perkin Elmer) after 20 min incubation at RT. Subsequently, Dual-Glo Stop & Glo Reagent diluted (1:100) in culture medium (Promega) was added to each well and the luminescence of the renilla luciferase was measured after

20 min incubation at RT. For data analysis, the Firefly luciferase signal was normalized to the renilla luciferase signal and statistical significance was determined through a t-test and plotted using Graph Pad Prism. All sequences for primers can be found in the Supplementary Table 2.

CRISPRi and CRISPRa in dCas9-U251-MG

Plasmid encoding Lenti-dCas9-KRAB-blast for CRISPRi was a gift from Gary Hon (Addgene plasmid #89567; http://n2t.net/addgene:89567) and the plasmid for CRISPRa was acquired from Addgene (plasmid #96917; https://www.addgene.org/96917/). The plasmids were packaged into a lentivirus and U251-MG were transduced with 200 µL of each virus. Two days later, blasticidin (Gibco) at a concentration of 10 µg/mL was supplied to the culture medium and cells were continuously kept under antibiotic selection and the resulting clonal cells are denoted as dCas9-KRAB U251-MG for CRISPRi and dCas9-VPR U251-MG for CRISPRa. Plasmids containing guide RNAs (gRNAs) against each target were produced and lentivirally packaged. After 10 days of selection with blasticidin (Gibco) containing medium, 200.000 dCas9-KRAB U251-MG or dCas9-VPR U251-MG cells were seeded into a 6-well plate. One day later, cells were transduced with 15 µL of viruses containing the gRNAs against each target. As controls, two different NT constructs for CRISPRi and one for CRISPRa and a *PRNP* targeting construct were used. After 72 hours for CRISPRi and 24 hours for CRISPRa, cell media was replaced with fresh medium containing 1 µg/mL puromycin (Gibco) to select for transduced cells. Cell media was replenished once more with puromycin containing medium and selection of transduced cells was terminated after a total selection duration of 5 days for CRISPRi and 3 days for CRISPRa in culture. Subsequently, cells were washed once in PBS and lysed for downstream analysis by TR-FRET and immunoblotting as well as quantitative real-time polymerase chain reaction (qRT-PCR). For TR-FRET and immunoblotting, cells were lysed by scraping in a total volume of 80 µL of lysis buffer (containing 50 mM Tris-HCl pH 8, 150 mM NaCl, 0.5% sodium deoxycholate, 0.5% Triton-X 100, Sigma) and processed for immunoblotting as described in this manuscript under the PUM1 validation subchapter. Same lysates were also used to quantitate PrP^C levels with a TR-FRET reaction with the same antibodies used for the screening. In detail, 10 µl of lysates were manually transferred to a 384-well opaque OptiPlate (Perkin Elmer) in quadruplicate wells and supplied with APC-POM1 and EU-POM2 (5 and 2.5 nM final concentration, respectively diluted in LANCE buffer). Plates were incubated overnight at 4°C followed by centrifugation and TR-FRET measurements were done with the same parameters used for the screening workflow. qRT-PCR was followed as described in the previous PUM1 validation section of this manuscript following the same protocol. For CRISPRi, each sample was measured for

three housekeeping genes (ACTB, GUSB and TBP) for normalization as well as their own respective primers to assess efficiency. For the final 9 hits, PRNP mRNA was assessed as well. For CRISPRa, each sample was measured for ACTB for normalization as well as their own respective primers to assess efficiency. qRT-PCR data was analyzed using the $2^{-\Delta\Delta CT}$ method and visualized using GraphPad Prism. All primer sequences are listed under Supplementary Table 2.

RNA-Sequencing in the U251-MG cell line

RNA extraction was performed using the RNeasy Mini Kit (Qiagen) according to the manufacturer's instructions. The libraries were prepared following Illumina TruSeq stranded mRNA protocol. The quality of the RNA and final libraries was determined using an Agilent 4200 TapeStation System. The libraries were pooled equimolecularly and sequenced in an Illumina NovaSeq6000 sequencer (single-end 100 bp) with a depth of around 20 Million reads per sample. The experiment was run in triplicates. For thresholding for non-expressed or low expressed genes before CRISPRi validation, first the average normalized counts for triplicates were calculated and a cut-off value of 25 was used (Supplementary Table 2).

Acknowledgements

AA is the recipient of an Advanced Grant of the European Research Council and grants from the Swiss National Research Foundation, the Nomis Foundation, the Swiss Personalized Health Network (SPHN, 2017DRI17), and a donation from the estate of Dr. Hans Salvisberg. We would like to thank Dr. Emilio Yangüez and Dr. Maria Domenica Moccia and the Functional Genomics Center Zurich (FGCZ) for their help with the RNA-Sequencing experiment. We thank Irina Abakumova and Rita Moos for their technical help.

Author Contributions:

Conceived and designed the experiments: DH, MA, AA. Supervised the study: SH, PH, AA. Contributions to experimental work; siRNA primary screen: DH, MA, DP, siRNA reformatting: DH, MA, DP, ME, siRNA secondary screen and CRISPRi/a experiments: DH, MA, bioinformatics: DH, MA, ES, AC, design and cloning of CRISPRi/a guides: JAY, AS, virus packaging, DH, MA, KM, experimental planning and development for smNPC-derived neurons: AD, smNPC-derived neuron experiments: AD, DH, MA, PUM1 experiments: DH, MA, BD, qPCR experiments: DH, MA, BD, ME. Wrote the paper: DH, MA, AA.

References

Aguzzi, A., and De Cecco, E. (2020). Shifts and drifts in prion science. Science *370*, 32-34.

Aguzzi, A., and Haass, C. (2003). Games played by rogue proteins in prion disorders and Alzheimer's disease. Science *302*, 814-818.

Andréasson, C., Ott, M., and Büttner, S. (2019). Mitochondria orchestrate proteostatic and metabolic stress responses. EMBO Rep *20*, e47865.

Ballmer, B.A., Moos, R., Liberali, P., Pelkmans, L., Hornemann, S., and Aguzzi, A. (2017). Modifiers of prion protein biogenesis and recycling identified by a highly parallel endocytosis kinetics assay. J Biol Chem *292*, 8356-8368.

Bellingham, S.A., Coleman, L.A., Masters, C.L., Camakaris, J., and Hill, A.F. (2009). Regulation of prion gene expression by transcription factors SP1 and metal transcription factor-1. J Biol Chem *284*, 1291-1301.

Bendheim, P.E., Brown, H.R., Rudelli, R.D., Scala, L.J., Goller, N.L., Wen, G.Y., Kascsak, R.J., Cashman, N.R., and Bolton, D.C. (1992). Nearly ubiquitous tissue distribution of the scrapie agent precursor protein. Neurology *42*, 149-156.

Bettayeb, K., Chang, J.C., Luo, W., Aryal, S., Varotsis, D., Randolph, L., Netzer, W.J., Greengard, P., and Flajolet, M. (2016). δ-COP modulates Aβ peptide formation via retrograde trafficking of APP. Proc Natl Acad Sci U S A *113*, 5412-5417.

Bohn, J.A., Van Etten, J.L., Schagat, T.L., Bowman, B.M., McEachin, R.C., Freddolino, P.L., and Goldstrohm, A.C. (2018). Identification of diverse target RNAs that are functionally regulated by human Pumilio proteins. Nucleic Acids Res *46*, 362-386.

Brandner, S., Isenmann, S., Raeber, A., Fischer, M., Sailer, A., Kobayashi, Y., Marino, S., Weissmann, C., and Aguzzi, A. (1996). Normal host prion protein necessary for scrapie-induced neurotoxicity. Nature *379*, 339-343.

Bueler, H., Raeber, A., Sailer, A., Fischer, M., Aguzzi, A., and Weissmann, C. (1994). High prion and PrPSc levels but delayed onset of disease in scrapie-inoculated mice heterozygous for a disrupted PrP gene. Mol Med *1*, 19-30.

Chen, S., Wang, R., Zheng, D., Zhang, H., Chang, X., Wang, K., Li, W., Fan, J., Tian, B., and Cheng, H. (2019). The mRNA Export Receptor NXF1 Coordinates Transcriptional Dynamics, Alternative Polyadenylation, and mRNA Export. Mol Cell *74*, 118-131.e117.

Dery, M.A., Jodoin, J., Ursini-Siegel, J., Aleynikova, O., Ferrario, C., Hassan, S., Basik, M., and LeBlanc, A.C. (2013). Endoplasmic reticulum stress induces PRNP prion protein gene expression in breast cancer. Breast Cancer Res *15*, R22.

Dhingra, A., Täger, J., Bressan, E., Rodriguez-Nieto, S., Bedi, M.S., Bröer, S., Sadikoglou, E., Fernandes, N., Castillo-Lizardo, M., Rizzu, P.*, et al.* (2020). Automated Production of Human Induced Pluripotent Stem Cell-Derived Cortical and Dopaminergic Neurons with Integrated Live-Cell Monitoring. J Vis Exp.

Dörrbaum, A.R., Kochen, L., Langer, J.D., and Schuman, E.M. (2018). Local and global influences on protein turnover in neurons and glia. Elife *7*.

Gilbert, L.A., Larson, M.H., Morsut, L., Liu, Z., Brar, G.A., Torres, S.E., Stern-Ginossar, N., Brandman, O., Whitehead, E.H., Doudna, J.A.*, et al.* (2013). CRISPR-mediated modular RNA-guided regulation of transcription in eukaryotes. Cell *154*, 442-451.

Hirst, J., Barlow, L.D., Francisco, G.C., Sahlender, D.A., Seaman, M.N., Dacks, J.B., and Robinson, M.S. (2011). The fifth adaptor protein complex. PLoS Biol *9*, e1001170.

Hopkins, P.C., Sáinz-Fuertes, R., and Lovestone, S. (2011). The impact of a novel apolipoprotein E and amyloid-β protein precursor-interacting protein on the production of amyloid-β. J Alzheimers Dis *26*, 239-253.

Jackson, A.L., Bartz, S.R., Schelter, J., Kobayashi, S.V., Burchard, J., Mao, M., Li, B., Cavet, G., and Linsley, P.S. (2003). Expression profiling reveals off-target gene regulation by RNAi. Nat Biotechnol *21*, 635-637.

Jackson, A.L., and Linsley, P.S. (2010). Recognizing and avoiding siRNA off-target effects for target identification and therapeutic application. Nat Rev Drug Discov *9*, 57-67.

Jones, E., Hummerich, H., Viré, E., Uphill, J., Dimitriadis, A., Speedy, H., Campbell, T., Norsworthy, P., Quinn, L., Whitfield, J.*, et al.* (2020). Identification of novel risk loci and causal insights for sporadic Creutzfeldt-Jakob disease: a genome-wide association study. Lancet Neurol *19*, 840-848.

Karapetyan, Y.E., Sferrazza, G.F., Zhou, M., Ottenberg, G., Spicer, T., Chase, P., Fallahi, M., Hodder, P., Weissmann, C., and Lasmezas, C.I. (2013). Unique drug screening approach for prion diseases identifies tacrolimus and astemizole as antiprion agents. Proc Natl Acad Sci U S A *110*, 7044-7049.
Kedde, M., van Kouwenhove, M., Zwart, W., Oude Vrielink, J.A., Elkon, R., and Agami, R. (2010). A Pumilio-induced RNA structure switch in p27-3' UTR controls miR-221 and miR-222 accessibility. Nat Cell Biol *12*, 1014-1020.
Kurata, M., Wolf, N.K., Lahr, W.S., Weg, M.T., Kluesner, M.G., Lee, S., Hui, K., Shiraiwa, M., Webber, B.R., and Moriarity, B.S. (2018). Highly multiplexed genome engineering using CRISPR/Cas9 gRNA arrays. PLoS One *13*, e0198714.
Kuzyk, A., Gartner, J., and Mai, S. (2016). Identification of Neuroblastoma Subgroups Based on Three-Dimensional Telomere Organization. Transl Oncol *9*, 348-356.
Küffer, A., Lakkaraju, A.K., Mogha, A., Petersen, S.C., Airich, K., Doucerain, C., Marpakwar, R., Bakirci, P., Senatore, A., Monnard, A.*, et al.* (2016). The prion protein is an agonistic ligand of the G protein-coupled receptor Adgrg6. Nature *536*, 464-468.
Mallucci, G.R., White, M.D., Farmer, M., Dickinson, A., Khatun, H., Powell, A.D., Brandner, S., Jefferys, J.G., and Collinge, J. (2007). Targeting cellular prion protein reverses early cognitive deficits and neurophysiological dysfunction in prion-infected mice. Neuron *53*, 325-335.
Millhauser, G.L. (2004). Copper binding in the prion protein. Acc Chem Res *37*, 79-85.
Minikel, E.V., Zhao, H.T., Le, J., O'Moore, J., Pitstick, R., Graffam, S., Carlson, G.A., Kriz, J., Kim, J.B., Ma, J.*, et al.* (2020). Prion protein lowering is a disease-modifying therapy across prion strains, disease stages, and endpoints. bioRxiv.
Muppirala, U.K., Honavar, V.G., and Dobbs, D. (2011). Predicting RNA-protein interactions using only sequence information. BMC Bioinformatics *12*, 489.
Owen, F., Poulter, M., Lofthouse, R., Collinge, J., Crow, T.J., Risby, D., Baker, H.F., Ridley, R.M., Hsiao, K., and Prusiner, S.B. (1989). Insertion in prion protein gene in familial Creutzfeldt-Jakob disease. Lancet *1*, 51-52.
Parkyn, C.J., Vermeulen, E.G., Mootoosamy, R.C., Sunyach, C., Jacobsen, C., Oxvig, C., Moestrup, S., Liu, Q., Bu, G., Jen, A.*, et al.* (2008). LRP1 controls biosynthetic and endocytic trafficking of neuronal prion protein. J Cell Sci *121*, 773-783.
Pease, D., Scheckel, C., Schaper, E., Eckhardt, V., Emmenegger, M., Xenarios, I., and Aguzzi, A. (2019). Genome-wide identification of microRNAs regulating the human prion protein. Brain Pathol *29*, 232-244.
Peters, H.L., Yan, Y., and Solheim, J.C. (2013). APLP2 regulates the expression of MHC class I molecules on irradiated Ewing's sarcoma cells. Oncoimmunology *2*, e26293.
Polymenidou, M., Moos, R., Scott, M., Sigurdson, C., Shi, Y.Z., Yajima, B., Hafner-Bratkovic, I., Jerala, R., Hornemann, S., Wuthrich, K.*, et al.* (2008). The POM monoclonals: a comprehensive set of antibodies to non-overlapping prion protein epitopes. PLoS One *3*, e3872.
PubChem, N. (2013). Ambion/Life Technologies whole genome siRNA sequence database.
Qi, L.S., Larson, M.H., Gilbert, L.A., Doudna, J.A., Weissman, J.S., Arkin, A.P., and Lim, W.A. (2013). Repurposing CRISPR as an RNA-guided platform for sequence-specific control of gene expression. Cell *152*, 1173-1183.
Raymond, G.J., Zhao, H.T., Race, B., Raymond, L.D., Williams, K., Swayze, E.E., Graffam, S., Le, J., Caron, T., Stathopoulos, J.*, et al.* (2019). Antisense oligonucleotides extend survival of prion-infected mice. JCI Insight *5*.
Roisman, L.C., Han, S., Chuei, M.J., Connor, A.R., and Cappai, R. (2019). The crystal structure of amyloid precursor-like protein 2 E2 domain completes the amyloid precursor protein family. FASEB J *33*, 5076-5081.
Rybner, C., Hillion, J., Sahraoui, T., Lanotte, M., and Botti, J. (2002). All-trans retinoic acid down-regulates prion protein expression independently of granulocyte maturation. Leukemia *16*, 940-948.
Shyu, W.C., Harn, H.J., Saeki, K., Kubosaki, A., Matsumoto, Y., Onodera, T., Chen, C.J., Hsu, Y.D., and Chiang, Y.H. (2002). Molecular modulation of expression of prion protein by heat shock. Mol Neurobiol *26*, 1-12.
Silber, B.M., Gever, J.R., Rao, S., Li, Z., Renslo, A.R., Widjaja, K., Wong, C., Giles, K., Freyman, Y., Elepano, M.*, et al.* (2014). Novel compounds lowering the cellular isoform of the human prion protein in cultured human cells. Bioorg Med Chem *22*, 1960-1972.
Stojic, L., Lun, A.T.L., Mangei, J., Mascalchi, P., Quarantotti, V., Barr, A.R., Bakal, C., Marioni, J.C., Gergely, F., and Odom, D.T. (2018). Specificity of RNAi, LNA and CRISPRi as loss-of-function methods in transcriptional analysis. Nucleic Acids Res *46*, 5950-5966.
Tamgüney, G., Giles, K., Glidden, D.V., Lessard, P., Wille, H., Tremblay, P., Groth, D.F., Yehiely, F., Korth, C., Moore, R.C.*, et al.* (2008). Genes contributing to prion pathogenesis. J Gen Virol *89*, 1777-1788.

Vallabh, S.M., Minikel, E.V., Schreiber, S.L., and Lander, E.S. (2020). Towards a treatment for genetic prion disease: trials and biomarkers. Lancet Neurol *19*, 361-368.
Van Etten, J., Schagat, T.L., Hrit, J., Weidmann, C.A., Brumbaugh, J., Coon, J.J., and Goldstrohm, A.C. (2012). Human Pumilio proteins recruit multiple deadenylases to efficiently repress messenger RNAs. J Biol Chem *287*, 36370-36383.
Vincent, B., Sunyach, C., Orzechowski, H.D., St George-Hyslop, P., and Checler, F. (2009). p53-Dependent transcriptional control of cellular prion by presenilins. J Neurosci *29*, 6752-6760.
Wulf, M.A., Senatore, A., and Aguzzi, A. (2017). The biological function of the cellular prion protein: an update. BMC Biol *15*, 34.
Zhang, J.H., Chung, T.D., and Oldenburg, K.R. (1999). A Simple Statistical Parameter for Use in Evaluation and Validation of High Throughput Screening Assays. J Biomol Screen *4*, 67-73.
Zhang, X.D. (2011). Illustration of SSMD, z score, SSMD*, z* score, and t statistic for hit selection in RNAi high-throughput screens. J Biomol Screen *16*, 775-785.

Supplementary materials

Supplementary Figure 1: Additional quality control of primary screening and establishment of siRNA treatment for smNPC-derived neurons.

A) Strictly standardized mean difference of each plate from the primary screening reporting the separation of the positive and negative controls. Range of the quality metrics (poor to excellent) is reported based on the highest level of stringency (Zhang, 2011). **B)** Endogenous PrP^C levels in human smNPCs and smNPC-derived neurons (day 11 post differentiation) assessed through immunoblotting. U251-MG was used as a positive control. The anti-PrP antibody POM2 was used for detection of PrP^C. **C)** Western blot analysis of 11 days old smNPC-derived neurons upon transfection with three distinct *PRNP* targeting siRNAs and a non-targeting siRNA as well as Lipofectamine only and untreated control. *PRNP* siRNA 1 and 2 lead to a marked decrease of PrP^C levels 6 days after transfection.

Supplementary Figure 2: Establishment, experimental setup and results of CRISPRi in dCas9KRAB-U251MG cells.

A) Efficacy of CRISPRi in dCas9-KRAB-U251-MG by lentivirally transduce a construct containing four single guides against *PRNP* as well as two non-targeting controls assessed through immunoblotting. After CRISPRi treatment followed by antibiotic selection for five days an evident reduction of PrP^C levels is apparent. **B)** Schematic depicting the setup of the CRISPRi experiments in dCas9-KRAB-U251-MG cells. **C)** Two candidates tested independently. PrP^C protein levels of dCas9KRAB-U251-MG cells transduced with gRNA CRISPRi lentiviruses against both targets. Mean values ± SD (n=4 technical replicates) are shown. CRISPRi activity measured by the mRNA level of the target gene in comparison to a negative control sample (NT1) after normalization to the housekeeping gene ACTB.

D) Panels depicting the on-target efficiency of CRISPRi downregulation on each target assessed by qRT-PCR five days post-selection, the effect of each target on *PRNP* mRNA levels in the same experiment and the effect of CRISPRi for all targets assayed on PrP^C levels.

Supplementary Figure 3: Establishment, experimental setup and results of CRISPRa in dCas9VPR-U251MG cells.

A) Schematic depicting the setup of the CRISPRa experiments in dCas9-VPR-U251-MG cells. **B)** Efficacy of CRISPRa in dCas9-VPR-U251-MG by lentivirally transduce a construct containing gRNAs against *PRNP* as well as a non-targeting control assessed through immunoblotting. **C**) Additional

quantification of B using TR-FRET. qRT-PCR of the same setup as in B. ΔCt values were normalized to those of *ACTB*. After CRISPRa treatment followed by antibiotic selection for three days an increase in PrP^C levels is apparent. **D)** CRISPRa efficiency for each gene measured by qRT-PCR after selection for three days. ΔCt values were normalized to those of *ACTB.* **E)** Effect of CRISPRa for all targets assayed on PrP^C levels measured by TR-FRET. **F)** Western blot analysis of representative samples from E. Antibody POM2 was used for detection of PrP^C. * $p \geq 0.05$, ** $p \geq 0.01$, **** $p \geq 0.0001$, n.s. = non-significant (Dunnett's multiple comparisons test).

Supplementary Table 1: Whole genome-RNAi screen results. Summary excel sheet for the primary screen dataset involving SSMD, log2fold change and p-values for each replicate. Second tab summarizing the 743 candidates that were validated in the secondary screening round.

Supplementary Table 2: RNA-Seq normalized counts for U251-MG.

Supplementary Table 3: Sequences of primers used in the study.

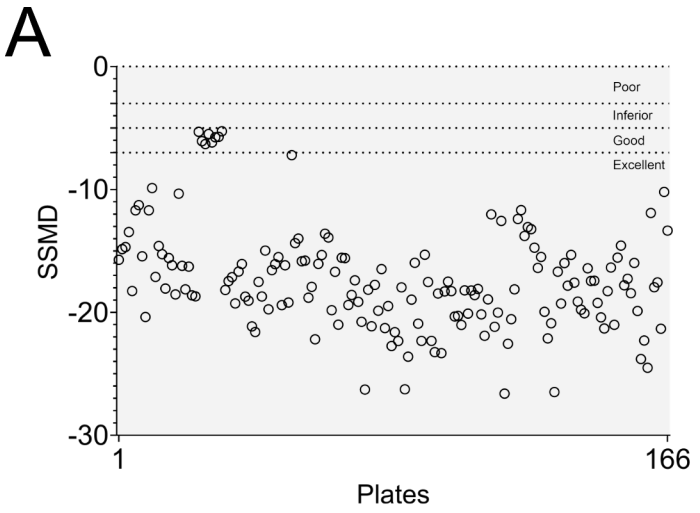

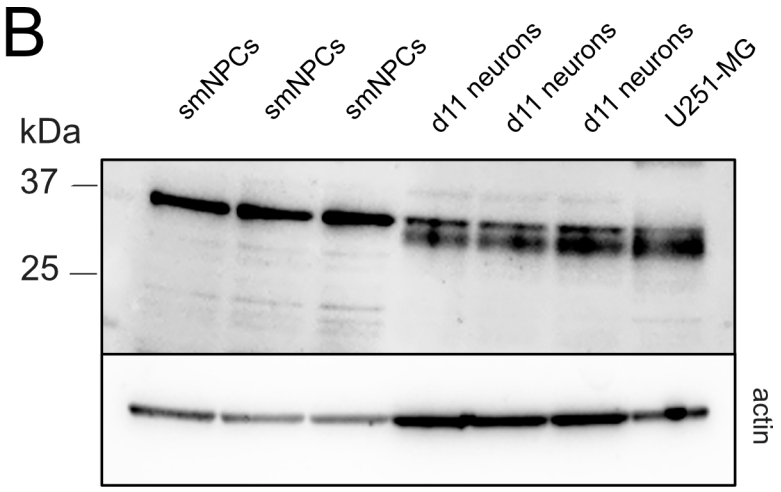

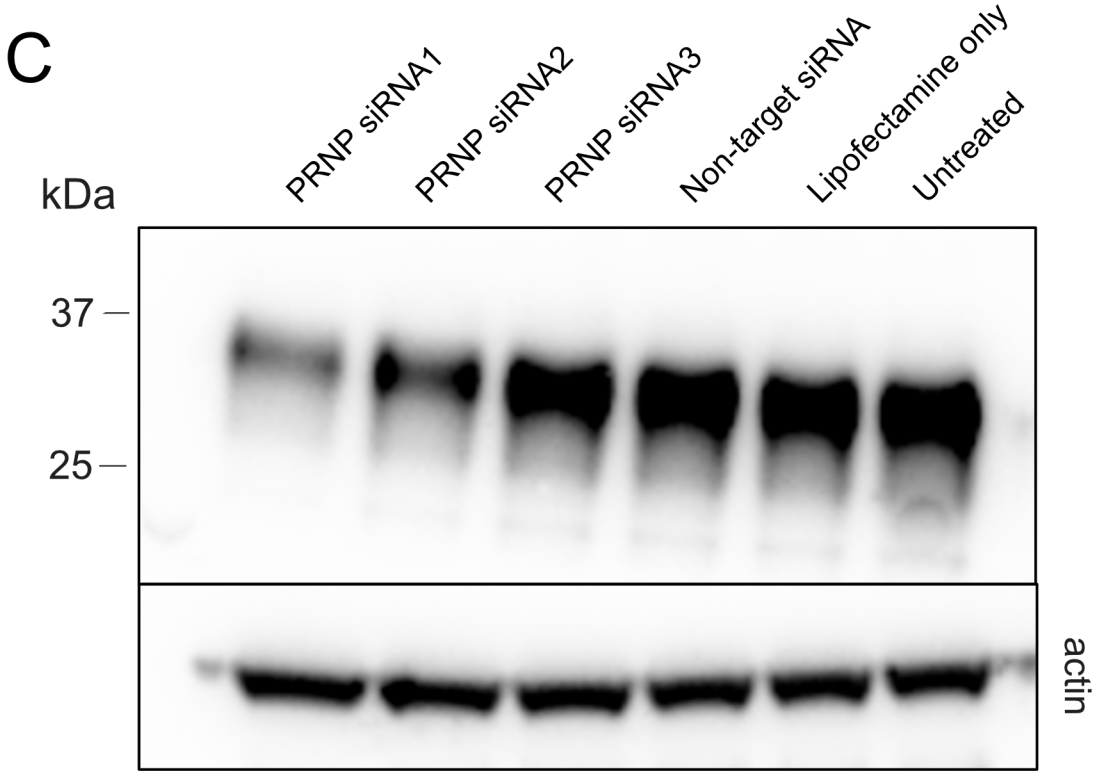

Heinzer, Avar et al., Supplementary Fig. 1

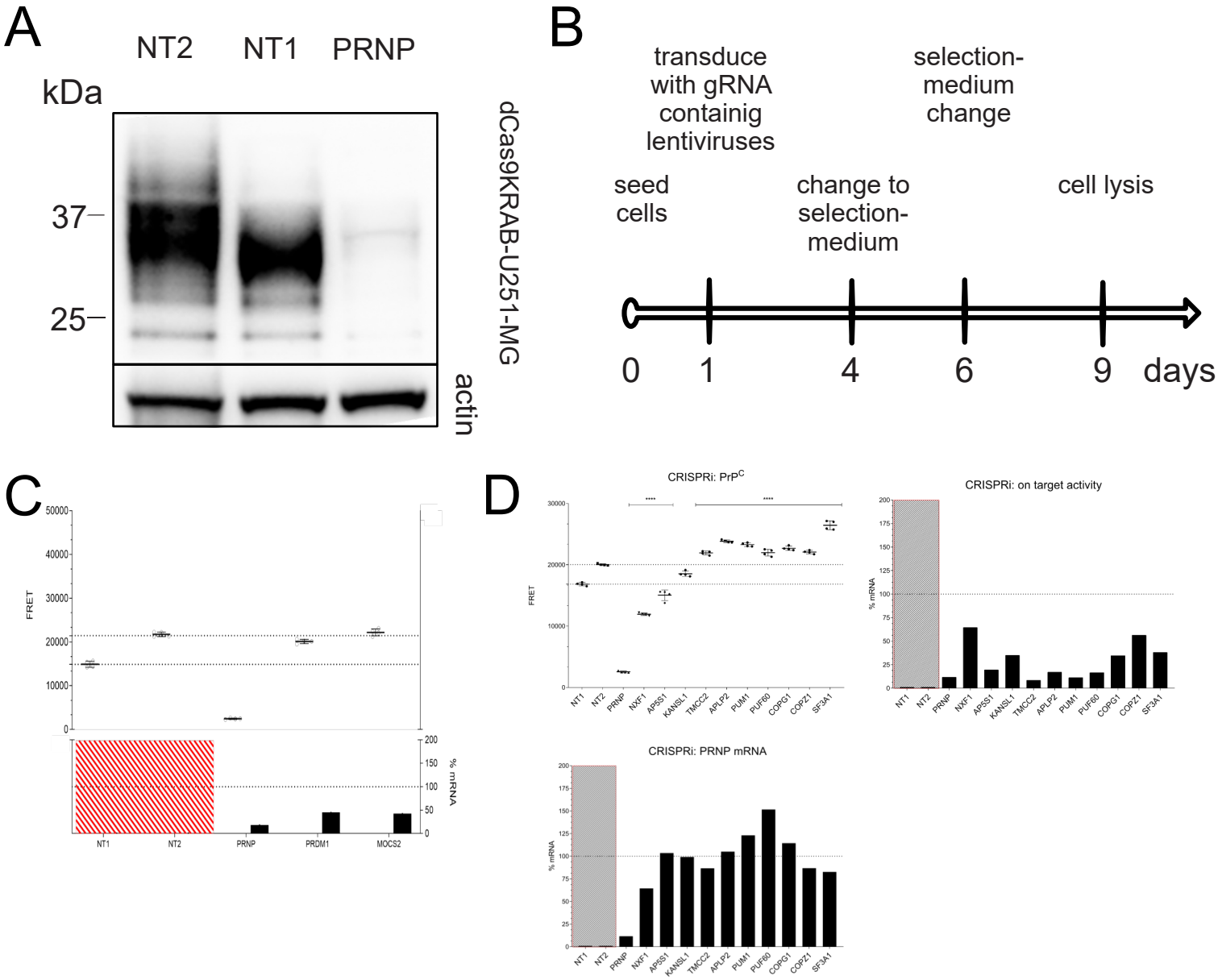

Heinzer, Avar et al., Supplementary Fig. 2

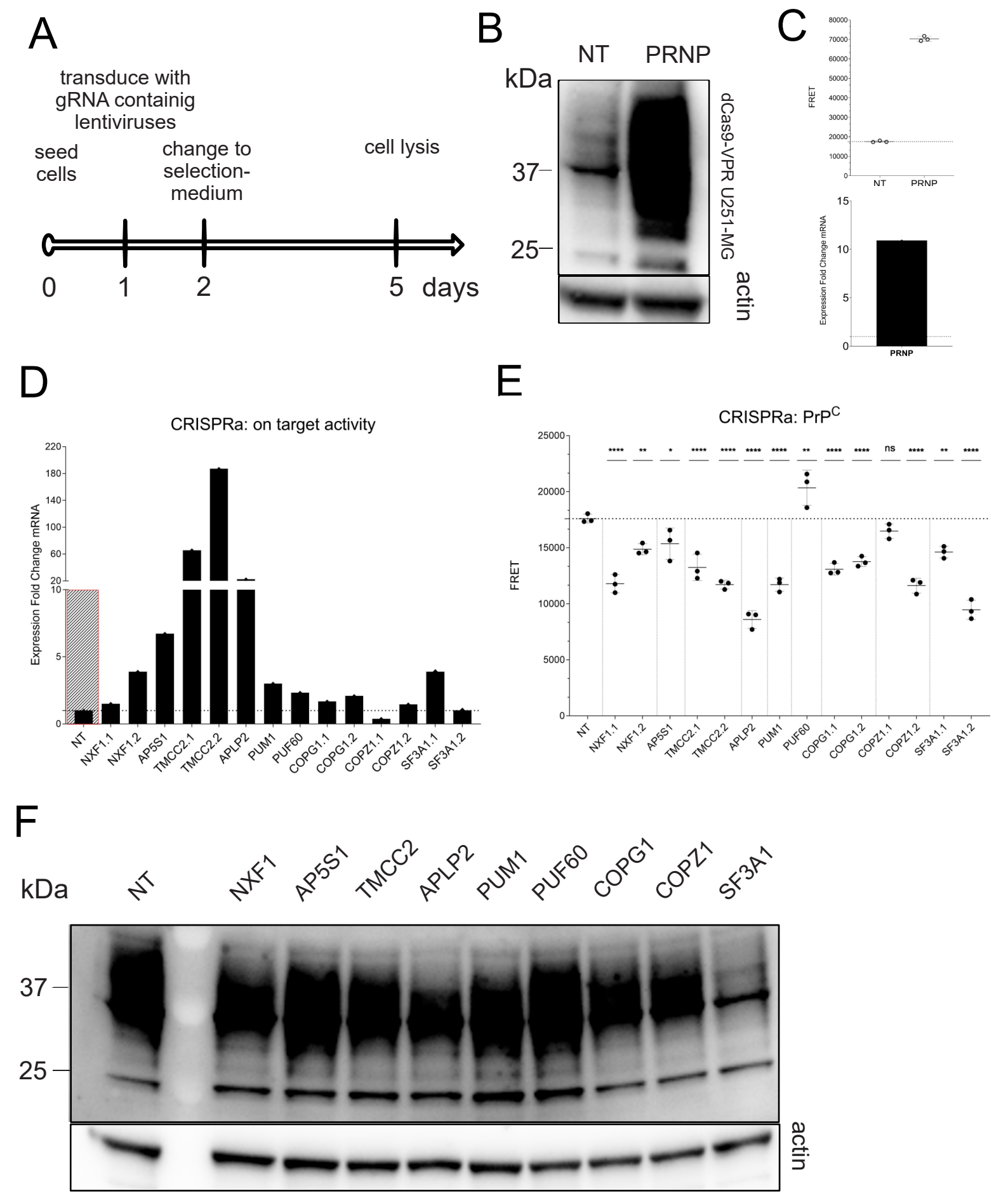

Heinzer, Avar et al., Supplementary Fig. 3